Pertanika J. Sci. & Technol. 30 (4): 2767 - 2788 (2022)

PERTANIKA JOURNALS

SCIENCE & TECHNOLOGY

Journal homepage: http://www.pertanika.upm.edu.my/

Comparative Computational Study of Double Rotating Cylinder Embedded on Selig S1223 Aerofoil and Flat Plate for High Altitude Platform

Hidayatullah Mohammad Ali*, Azmin Shakrine Mohd Rafie, Mohd Faisal Abdul Hamid and Syaril Azrad Md. Ali

Department of Aerospace Engineering, Faculty of Engineering, Universiti Putra Malaysia, 43400 Serdang, Selangor, Malaysia

ABSTRACT

The high-altitude platform was built as an alternative approach to address the weakness of the terrestrial and satellite communication networks. It can be an aircraft or balloon positioned 20 to 50 km above the earth's atmosphere. The use of the Magnus effect was not noticeable in the production of the high-altitude platform, while past research study has denoted its aerodynamic performance in generating greater lift and stall angle delay, which would be beneficial in creating such a flying device. This research delineates the proposed designs using the computational fluid dynamics approach utilizing ANSYS WORKBENCH 2019 software. The embedment of the rotating cylinder onto the design would best portray the use of the Magnus effect in generating higher lift coefficients with probable delay in stall angle. Hereby, the design of embedding rotating cylinder onto Selig S1223 aerofoil and the flat plate is proposed to test their aerodynamic performances for high altitude platform purposes. Here, Fluent fluid flow analysis was simulated for 500 RPM and 1000 RPM momentum injection with free stream velocities from 5 m/s to 30 m/s for different angles of attack of 0 to 20 degrees. The analysis has resulted in a greater impact on its lift coefficient and stall angle delay of about 39% and 53% enhancement for modified aerofoil while showing 128% and 204% betterment for modified flat plate than their respective unmodified model. Therefore, it is perceived that the CyFlaP has better stability yet is simplistic in a design suitable for HAP application.

Keywords: Computational fluid dynamic, flat plate, high altitude platform, rotating cylinder, Selig S1223 aerofoil

ARTICLE INFO

Article history:
Received: 20 November 2021
Accepted: 07 March 2022
Published: 23 September 2022

DOI: https://doi.org/10.47836/pjst.30.4.26

E-mail addresses:
hidayatmaddali@gmail.com (Hidayatullah Mohammad Ali)
shakrine@upm.edu.my (Azmin Shakrine Mohd Rafie)
mohd_faisal@upm.edu.my (Mohd Faisal Abdul Hamid)
syaril@upm.edu.my (Syaril Azrad Md. Ali)
* Corresponding author

ISSN: 0128-7680
e-ISSN: 2231-8526

INTRODUCTION

The high-altitude platform (HAP) has attracted constant growth of interest internationally for the past few years. It is a new concept of infrastructure which can be easily deployed to support the current or existing systems. It was built as an alternative approach to address the weakness of the terrestrial and satellite communication networks. Simultaneously, the existing infrastructure's restrictions and disadvantages can be devoid of the application of HAP. HAP can be an aircraft, balloon, or airship positioned 20 km to 50 km above the earth and intended to provide surveillance, terrestrial, and telecommunication services (Gultom, 2016). It greatly gives an advantage of the ease of placement, low operating costs, low propagation delay, wide elevation angle, wide coverage. Moreover, it can be used for broadband services, broadcasts, and disastrous conditions. The HAP is available worldwide where several projects have been and are being conducted in the United States, Europe, and Asia involving national space agencies such as the National Aeronautics and Space Administration (NASA), the European Space Agency (ESA), the German Aerospace Center (DLR), the Korea Aerospace Research Institute (KARI), and the Japan Aerospace Exploration Agency (JAXA) (Fidler et al., 2010).

Furthermore, HAP is quasi-stationary vehicles that operate in the stratosphere region, which falls well above the clouds, civil air routes, and jet streams, but below the mesosphere and thermosphere region (Fidler et al., 2010; Tozer & Grace, 2001). Chunchuzov et al. (2015) denoted that the wind velocity in this region may go up to 10 m/s per 100 m and beyond. The relatively low wind speed and turbulence make it perfect for this region, so air navigation has no problems. However, it is important to note that the former design of the HAP is large to fly at such extreme operating conditions of height and wind speed. Based on history, the size of the HAP ranges from 23 m up to 305 m in length, and none incorporates the Magnus effect in their design despite the well variant of its high lift generation (D'Oliveira et al., 2016).

In 1997, Modi studied Magnus effect embedment onto different configurations on a symmetrical aerofoil and thus resulted in a tremendous effect on its aerodynamic coefficients (Modi, 1997). The researcher denoted that a rotating cylinder application onto the model proves that it improves the lift capability over the ranges of low to a medium angle of attack (α). Furthermore, Ahmed et al. (2014) have conducted a numerical assessment of such embedment for NACA 0024 aerofoil, which has revealed an improvement in lift coefficient (C_L) and stall angle delay of 36% and 122%, respectively, compared to its unmodified model. Following this, the numerical analysis by Huda et al. (2015) incorporated a leading-edge rotating cylinder onto the NACA 0010 aerofoil at a rotational speed of 30, 60, 90, and 120 RPM, thereby generating a surprising improvement in the maximum lift of 145% in comparison with the unmodified NACA 0010 aerofoil model. Similarly, Faisal et al. (2017) have undertaken experimental and numerical analyses both by applying the

leading-edge rotating cylinder onto NACA 0018. However, the scholars did not record the pre- and post-aerodynamic characteristics of the modified aerofoil. Additionally, Salam et al. (2019) studied the effect of rotating cylinder on NACA0021 and discovered an increase in C_L and reduction in drag coefficient (C_D) for all α. Furthermore, a delay in flow separation was also viewed at higher α in view of momentum injection by the leading-edge cylinder.

The rotating cylinder embedment onto the bluff body occurred in 1925 (Wolff, 1925). Following this, studies pertaining to cylinder embedment on the flat plate (CyFlaP) are usually influenced by the past research known as leading edge cylindrical aerofoil (LECA). In comparison, the research on the bluff body has only come into the picture within the last decade where the cylinder to bluff body configuration was experimentally studied by Modi et al. (1991) but based only on drag reduction for automotive purposes. Accordingly, the researcher denoted that configuration resulted in a reduction of 75% in C_D. Wang et al. (2013) investigated the use of flat plates in 2013 when they examined the flat plate configuration for its aerodynamic coefficient. At around 60% of the maximum lift coefficient (C_{Lmax}), they denoted that the flat plate could generate a high coefficient at higher α.

Therefore, this paper delineates two (2) proposed designs for the preliminary design of the HAP. First, the design of a rotating cylinder onto 1) Selig S1223 aerofoil and 2) flat plate are proposed. A two-dimensional flow testing has been simulated by using the Computational Fluid Dynamic (CFD) approach utilizing a Fluent analysis system from the ANSYS WORKBENCH 2019 Software for momentum injection of 500 and 1000 revolution per minute (RPM) with free stream velocities ranging from 5 m/s to 30 m/s for different α of 0 to 20 degrees (°). Finally, the model is proposed to study its efficiency for aerodynamic generation purposes.

This study is a novel concept incorporating a new embedment of rotating cylinder onto Selig S1223 aerofoil and flat plate intended for HAP purposes. It can be used as a future reference and benchmark for designing HAP. The novelty of embedding such aerodynamic and bluff bodies together would further elevate the aerospace industry to explore such an objective sense. In addition, the results from this CFD simulation may be of interest to the CFD community for numerical studies that consider the Magnus effect in the same class of flow regions.

METHODOLOGY

The methodology is comprised of several subsections and thus offers an insight into the research flow for the study.

Geometry and Computational Modelling

The design parameters of the model were the most important consideration that had to be considered in this study. Therefore, a thorough study of the past research data has thus

implemented onto the CFD software. An embedment of rotating cylinder onto 1) Selig S1223 aerofoil and 2) flat plate are proposed. The design parameter was posed for the available resource data as follows.

Cylinder. In 2008, Badalamenti tested a rotating cylinder in the Handley Page Laboratory of Aerodynamics at City University by utilizing a wind tunnel (Badalamenti & Prince, 2008). For the effects of the rotating cylinder, he demonstrated the aerodynamic properties, which were then applied in comparison to other configurations from previous research. He also verified the data obtained by showing agreement with Betz's analysis for the same aspect ratio (AR) of 4.7 (Barati et al., 2019). The formula used for the aspect ratio is Equation 1:

$$AR = \frac{b}{c} = \frac{b}{c} * \frac{b}{b} = \frac{b^2}{A} \quad [1]$$

Where b is the span of the cylinder, c is the chord, and A denotes the model area. Accordingly, the calculations and the formulas used were fully integrated for the study. Therefore, the data incorporated will be used for validation in a later subsection (refer to subsection 2.6). According to Badalamenti & Prince's study (2008), the cylinder's dimension was set at AR = 5.1, corresponding to a diameter (Ø) of 0.16 m, as shown in Figure 1. Duly noted that the cylinder is rotating clockwise, opposing the relative velocity to mimic the same condition (Badalamenti & Prince, 2008). Furthermore, Barati et al. (2019) have done the same concept over the clockwise rotation of the cylinder to aid the freestream flow on top of the cylinder while having the one at the bottom opposing it. Therefore, it ensures an upward force for the generated lift. For 2D planar simulations, the geometry is displayed as an XY plane, and the Z-axis is oriented away from the computer screen. Hence, a counterclockwise rotation is denoted as positive and clockwise rotation is negative based on the right-hand thumb rule. Therefore, the inserted value should be input as -500 or -1000 RPM (clockwise rotation) speed for the moving wall with the rotational motion for the cylinder's wall.

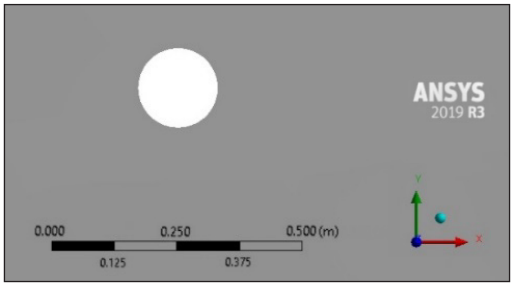

Figure 1. The geometry of the cylinder

Selig S1223 Aerofoil. The Selig S1223 aerofoil is well known for its high lift generation at a low Reynolds number (Re), originally patented by Michael S. Selig in 1995 (Selig et al., 1995). In addition, Oller et al. (2016) used the aerofoil in their study to test for hydrofoils' effectiveness and obtained a tremendous effect for such fluid conditions. He further noted that the aerofoil yielded high separation flow aftward at high α. As a result, the LECA is investigated to determine the aerodynamic profile of such embedment.

Ergo, the aerofoil was an upscale version of the original one with a ratio of 1:1.45 from the unmodified model to meet the performance objective of the study (Figure 2). Validation of the unmodified aerofoil has been performed and is displayed in the next subsection in comparison to the experiment performed by Selig et al. (Selig et al., 1995; Selig et al., 1996).

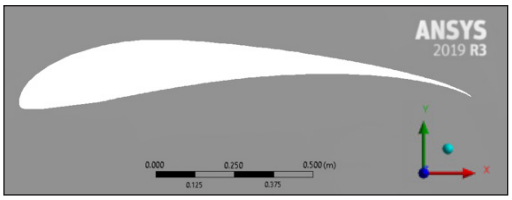

Figure 2. The geometry of the Selig S1223 aerofoil

LECA. The LECA design was presented in Figure 3, with a rotating cylinder embedded at the leading and trailing edges of the Selig S1223 aerofoil. This double embedment onto the aerofoil was adopted as per the study by Modi, where he incorporated several configurations of rotating cylinders onto a symmetrical aerofoil in 1997 (Modi, 1997). Therefore, the researcher's work inspired the creation of such a design, which was then used in this LECA investigation. The embedment was set up along the camber line of the aerofoil while maintaining a gap of 0.005 m between the cylinder and the aerofoil. The gap was set to optimum configuration performance for the model's embedment (Abdulla & Hasan, 2018). The embedment of the cylinder at 3/20 of the camber line was utilized to optimize its diameter to fit the aerofoil's leading edge and trailing edge, and thus satisfied with the experimental data by Michael S. Selig and James Gugliemo (Selig & Guglielmo, 1997).

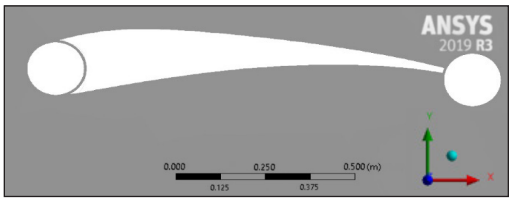

Figure 3. The geometry of the LECA

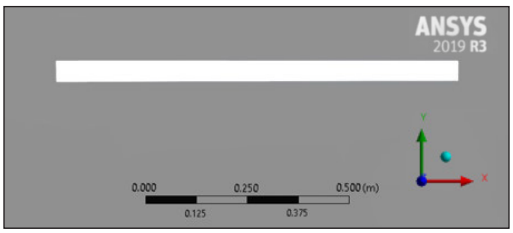

Figure 4. The geometry of the flat plate

Flat Plate. Another design that incorporates and utilizes the flat plate was developed to provide a simpler HAP design that can be compared to the LECA. The flat plate design by Torres (2002) and Wang et al. (2013) was duly referred on its capability for a flight at a higher value of α. As a result, the flat plate relevant to the researcher's study was established with a flat plate length of 1.00 m, as illustrated in Figure 4.

CyFlaP. The idea of the design for the CyFlaP would not spark without knowing its existence which was first introduced in 1997 by Modi (Modi, 1997). At that moment, Modi was simply testing the concept for its drag reduction for a vehicle instead of its

lift generation. Therefore, the design will be used for the CyFlaP with dual cylinder embedment at both the flat plate leading edge and trailing edge, as shown in Figure 5. A gap of 0.005 m was always enforced between the cylinder and the flat plate.

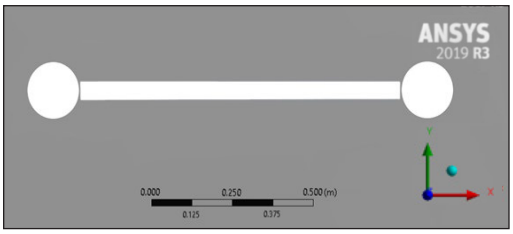

Figure 5. The geometry of the CyFlaP

Turbulence Model

Turbulence modeling, by definition, denotes a numerical technique designed to close a system of mean flow equations. It defines the design and usage of mathematical models to solve and simulate turbulence impacts, whereby their turbulence equations also provide simpler solutions using the averaging method. Turbulence modeling differs in the way they are calculated by extending the Navier-Stokes equations with additional terms consisting of some parameters such as local fluid velocity, wall distance, additional transport equations, eddy viscosity, turbulent kinetic energy, turbulence intensity, and others. Here, the Spalart-Allmaras, K-epsilon (K-ε), and K-omega (K-ω) models are some of the turbulence models that are often used in applications (Monk & Chadwick, 2017).

Spalart-Allmaras model is a one equation model which solves its modeled transport equation for the kinematic eddy viscosity (Kim et al., 1999). This model has produced promising results in simulation that involves wall-bounded flows. Moreover, it produces excellent results for boundary layers subjected to adverse pressure gradients, especially the one that occurs during vortex separation and turbulent flows over the wing surfaces (Kölzsch & Breitsamter, 2014). However, the model is less sensitive to numerical errors when non-layered meshes are used near the walls. The near-wall gradients of the transported variable used in this model are far smaller than in the K-ε and K-ω.

The K-ω model was used for the current work with reference to the study by Mgaidi et al. (2018), which implemented two extra transport equations as a two-equation model to delineate the turbulent flow properties accordingly. Hence, the turbulent kinetic energy is referred to as K as the first variable transported, while the second transported variable is referred to as ω. However, it has difficulty converging and relies on an initial estimation at the beginning of the solution. Therefore, it is common in the industry to use the K-ε model first, where the kinetic energy dissipation rate is solved. However, the K-ω model is far more suitable for obtaining accurate results in many aerodynamic situations, especially for highly curved and separated flows (Ali et al., 2021a; Ali et al., 2021b; Mgaidi et al., 2018; Monk & Chadwick, 2017).

Antecedent to this, Menter developed a two-equation eddy-viscosity model, otherwise referred to as the SST K-ω turbulence model, which is used in the near-wall region to combine and blend with the SST K-ω model in the far-field free stream K-ω model (Menter,

1994). The model is an advanced extension of the original model proposed by Wilcox in 1988, which can demonstrate a strong turbulence formulation for both the adverse pressure gradients and the separating flow (Wilcox, 1988). Conversely, the SST formulation is built by the integrated modeling of the K-ω and K-ε formulations, whereby the amalgamation helps the SST in transitioning from the K-ω model to the K-ε model to prevent problems occurring in the inlet of the free-stream turbulence (Mgaidi et al., 2018). At the same time, the K-ω formulation is included in the inner portion of the boundary layer instead of its K-ε equivalent. Consequently, the general form of transport equations in the Fluent analysis system is as shown in Equations 2 and 3:

$$\frac{\partial}{\partial t}(\rho k) + \frac{\partial}{\partial x_i}(\rho k u_i) = \frac{\partial}{\partial x_j}\left[\Gamma_k \frac{\partial k}{\partial x_j}\right] + G_k - Y_k + S_k \quad [2]$$

$$\frac{\partial}{\partial t}(\rho \omega) + \frac{\partial}{\partial x_i}(\rho \omega u_i) = \frac{\partial}{\partial x_j}\left[\Gamma_\omega \frac{\partial \omega}{\partial x_j}\right] + G_\omega - Y_\omega + S_\omega \quad [3]$$

The generation of turbulence kinetic energy due to mean velocity gradient and output of ω is expressed in these equations as G_k and G_ω, respectively. Meanwhile, the effective diffusivity of k and ω due to turbulence is expressed as Γ_k and Γ_ω, respectively. The dissipation of k and ω is then presented as Y_k and Y_ω, respectively, whereas the D_ω presents the cross-diffusion concept. Finally, yet importantly, the S_k and S_ω are the input by the user-defined source terms.

Concerning the above argument, the SST K-ω model is identical to the standard K-ω model but contains the following refinements (Ali et al., 2021a; Khalil et al., 2018):

(a) A blending function feature is used to multiply the standard K-ω model with the transformed K-ω model, which is then applied or added together.
(b) In the blending function, the standard K-ω will be triggered for a near-wall region, while the transformed K-ω will be activated zero away from the surface.
(c) The ω equation in the SST model is derived as a dampened cross-diffusion.
(d) The discrepancy between the turbulent shear stress transport and the modeling constant is compensated for by adjusting the turbulent viscosity definition.

All these refinements will allow the SST K-ω model to be extremely effective and efficient for a wider variety of flows, including aerofoils, adverse pressure gradient flows, and transonic shock waves, relative to the standard K-ω model (Khan et al., 2020). Therefore, the research study will mainly implement the SST K-ω model, which allows the model to be directly used on the wall through the viscous sublayer. Many who have worked with this particular model have found that promising results have been obtained in situations with adverse pressure gradients and separating flows (Ali et al., 2021a; Ali et al., 2021b; Hamisu et al., 2019; Mgaidi et al., 2018; Monk & Chadwick, 2017).

Key Performance Parameter

This study's Key Performance Parameters (KPPs) directly and precisely describe the output target. Here, the C_L and C_D equations used for the model formulation are presented in Equations 4 and 5.

$$C_L = \frac{L}{\frac{1}{2} * \rho * V^2 * S} \quad [4]$$

$$C_D = \frac{D}{\frac{1}{2} * \rho * V^2 * S} \quad [5]$$

where L is the lift force, D is the drag force, ρ is the density of the fluid (i.e., air), V is the free stream velocities, and S is the projected area of the model.

Grid Generation

The standard CFD process will need a mesh appropriate for the computational domain boundaries. It involves the generation of a computational mesh appropriate for the expected 2D Navier-Stokes equations, in which a set of grid points are defined for the domain and its boundaries. A grid structure like this is referred to as grid generation.

Mesh Topology. Two meshing zones were integrated into the Fluent fluid flow analysis system. The domain consists of an inner zone with a block of 2Ø × 3Ø around the model and an outer zone with a block setup of 6Ø × 15Ø across the inner zone [Figures 6(a) and 6(b)]. The block setup was applied based on the research work of Mgaidi et al. (2018) and Yao et al. (2016). The LECA and the CyFlaP models use the identical domain configuration throughout the investigation. The model surfaces were fixed with y-plus (y+) less than 1, which was located from the

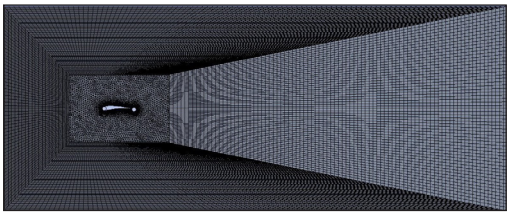

(a)

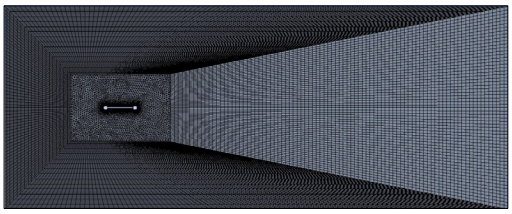

(b)

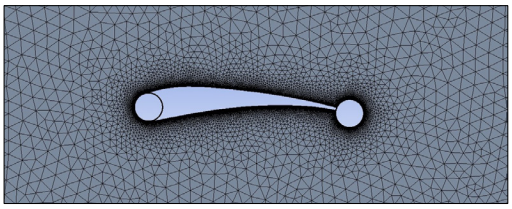

(c)

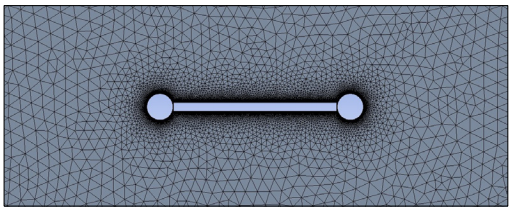

(d)

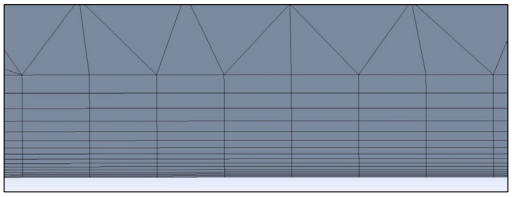

(e)

Figure 6. Domain and mesh generation for the LECA and CyFlaP model, from the domain setting for LECA (a) and CyFlaP (b), mesh generated for LECA (c) and CyFlaP (d), to the inflation set up on the model (e)

wall to the first mesh node in compliance with the inflation criterion of a maximum of 10 layers and with a growth rate of 1.2 to obtain good results [Figures 6(c), 6(d) and 6(e)]. This y+ is a non-dimensional distance often used to determine how fine or coarse a mesh is for a particular flow pattern. It is a ratio between laminar and turbulent influence in a cell. Here, it was used to determine the proper size of the cells near its domain walls which were important in turbulence modeling. A faster flow near the wall will produce higher values of y+, so the grid size near the wall must be reduced. Therefore, an inflation layer between 10 and 15 layers on the domain wall will generally resolve the boundary layer and accurately predict any separation or reattachment points. In addition, the wall function strategy could be conveniently achieved for a particular turbulence model. The specifications of the boundary conditions and mesh environment for this analysis are provided, as per Tables 1 and 2.

Table 1
Specifications of boundary conditions

Boundary conditions	**Type**
Inlet	Velocity-inlet
Outlet	Pressure-outlet
Cylinder	Wall
Cylinder Aftward	Wall
Selig aerofoil	Wall
Flat Plate	Wall
Wall	Symmetry
Interior surface body	Interior
Surface body	Interior

Table 2
Mesh configurations

Mesh specifications	
Growth rate	1.2
Defeature size	5.e-004 m
Curvature minimum size	1.e-003 m
Curvature normal angle	18.0°
Smoothing	High
Inflation specifications	
Inflation option	First layer thickness
First layer height	1.e-005 m
Maximum layers	10
Growth rate	1.2

Mesh Independency Test. In order to monitor the solution grid independence before commencing with the model testing phase, a mesh independency test (MIT) was recommended (Abdulla & Hasan, 2018). It was obtained by establishing a new cell grid and testing it utilizing various alternatives. Ergo, as seen in Figures 7 and 8, MIT is conducted for the LECA and CyFlaP to obtain the best data quality. Consequently, at approximately 1.560e+005 (LECA) and 1.640e+005 (CyFlaP) cells, the grid refinement for C_L resulted in the highest accuracy and durability for CFD research from now on. At this point, the simulation solves time was denoted with an increase of elements where the system's response converges to a solution where further refinement of the mesh would not affect the solution. Therefore, refinement past this intersection point is an inefficient application of CFD; hence the selected number of cells would be appropriate in capturing the system behavior while reducing the solve time. The percentage error from the described grid refinement was less than 1% to achieve the optimal time efficiency.

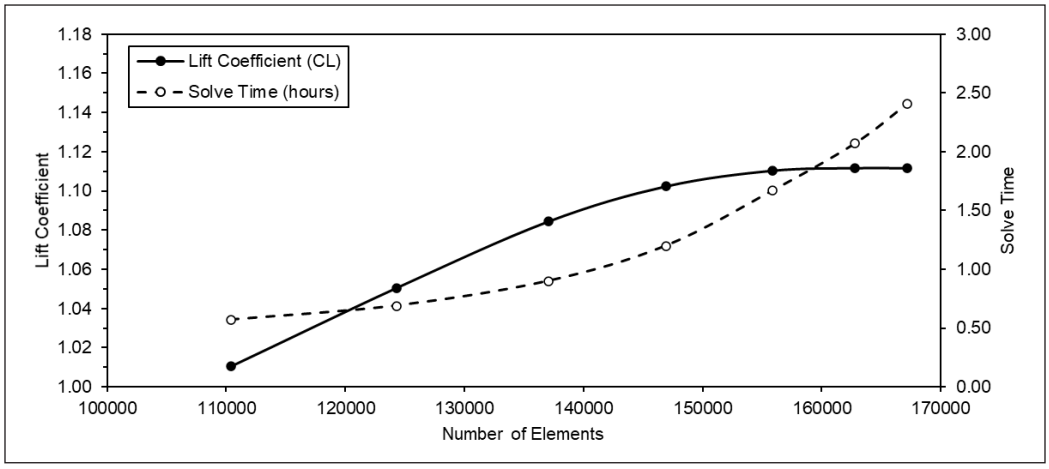

Figure 7. MIT for the LECA's convergence versus solve time

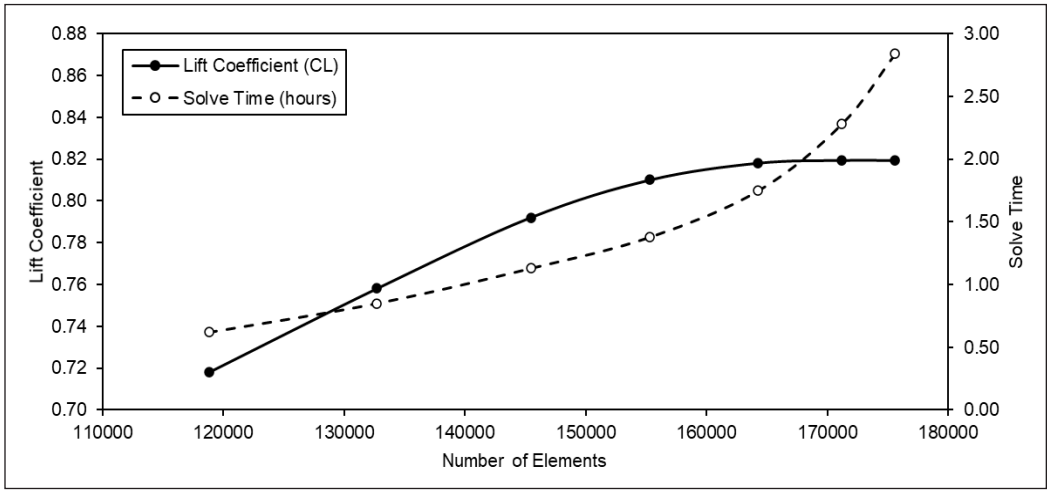

Figure 8. MIT for the CyFlaP's convergence versus solve time

Solver Setting

Before beginning the simulation solutions, it is critical to specify the settings for the targeted condition in the CFD solver interface. The best setup was introduced to evaluate the computational simulations, as seen in Table 3.

Validation

Validation for the cylinder, Selig S1123 aerofoil, and the flat plate was studied to obtain better results before starting deeper through the CFD process. The validation method has been referred to based on a few research as a guidance for the validation used (Boye et al., 2017; Gowree & Prince, 2012; Merryisha & Rajendran, 2019; Salam et al., 2019). Based

Table 3
ANSYS Fluent 19 solver setting

General	
Type	Pressure-based
Velocity formulation	Absolute
Time	Transient
2D space	Planar
Model	
Viscous	SST k-omega
Reference values	
Density (kg/m3)	1.225
Pressure (pascal)	101325
Temperature (K)	288.16
Velocity (m/s)	5,10,15,20,25,30
Viscosity (kg/m-s)	1.789e-005
Turbulence	
Specification method	Intensity and length scale
Turbulent intensity (%)	5
Turbulent length scale (m)	9.310e-002
Solution	
Method	Pressure-velocity coupling
Scheme	Coupled
Residual error	1.e-006
Spatial discretization	
Gradient	Green Gauss Node Based
Pressure	PRESTO!
Momentum	QUICK
Turbulent kinetic energy	QUICK
Specific dissipation rate	QUICK
Transient formulation	Bounded Second Order Implicit

on this validation analysis, the embedment of the LECA and CyFlaP was cautiously carried out. Badalamenti and Prince (2008), Torres (2002), and Selig et al. (1995) performed experimental fluid dynamics (EFD) on the rotating cylinder, Selig S1223 aerofoil, and flat plate, which were then validated by using the CFD approach, as illustrated in Figures 9 to 11. The validation analysis for each of the situations culminated in an error of less than 10%.

RESULTS AND DISCUSSION

The numerical results were obtained for flow over the proposed LECA and CyFlaP embedment for free stream velocities of 5 m/s up until 30 m/s at different α (i.e., 0°, 5°, 10°, 15°, and 20°) and for a rotational speed of 500 RPM and 1000 RPM. For LECA and CyFlaP conditions, a gap of 0.005 m was set between the cylinder, the aerofoil and/

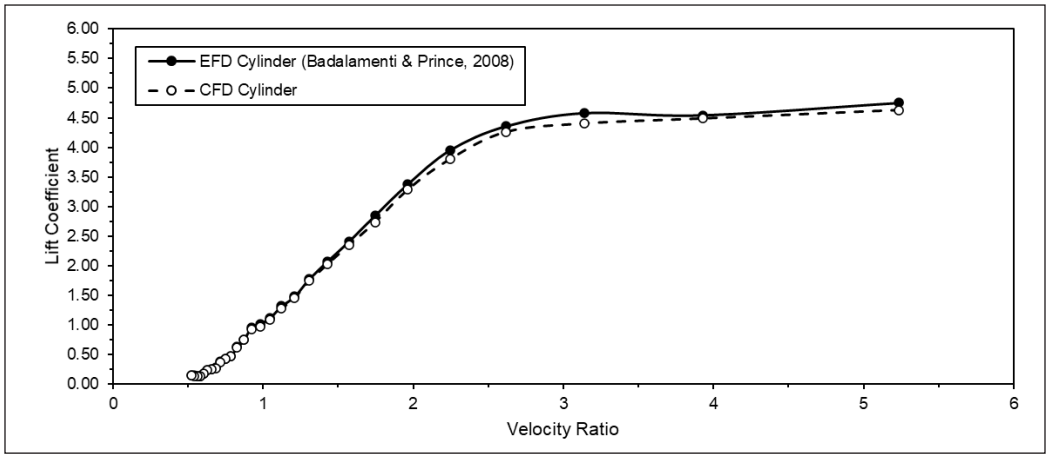

Figure 9. Validation of rotating cylinder

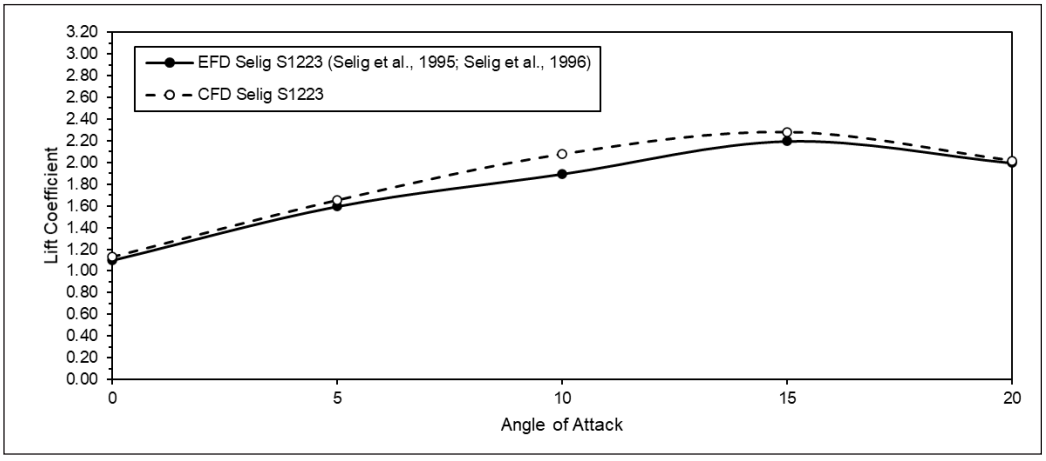

Figure 10. Validation of Selig S1223 aerofoil

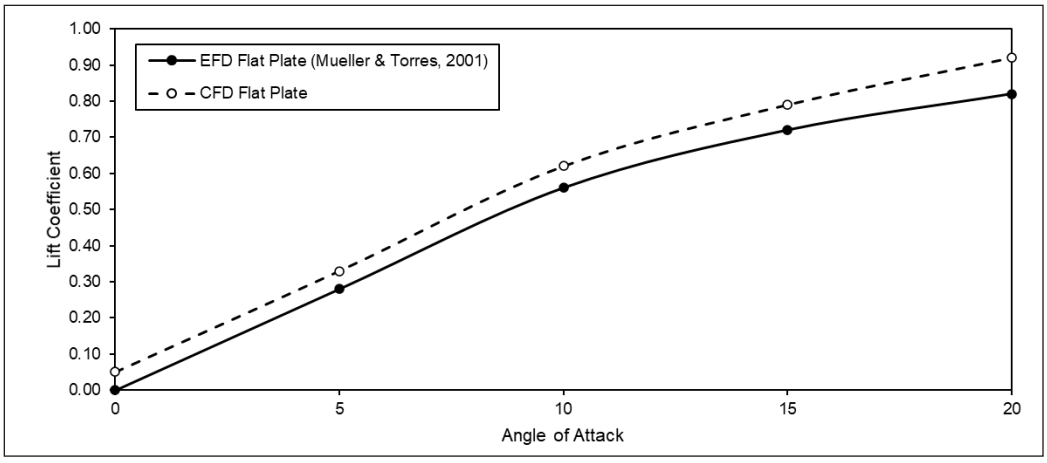

Figure 11. Validation of flat plate

or flat plate. Additionally, it is often necessary to estimate the turbulent intensity on the inlet when setting boundary conditions for a CFD simulation. For simulations at this class of stratosphere flow region in which the inlet involves a turbulent boundary layer for wall-bounded flows, the inlet turbulent intensity level is set to the recommended default "Medium," which is 5%, together with its turbulent length scale of 9.310e-002, respectively (ANSYS, 2013; Šidlof et al., 2017; Russo & Basse, 2016).

Numerical Simulation

In compliance with the following clauses, the numerical simulation was specified accordingly. As a result, the aerodynamic flow analysis is dominated by the dimensionless parameters C_L, C_D, RPM, Re, and α, resulting in a functional relationship with the numerical solution's performance.

Effect of Magnus Effect. As shown in Figures 12 to 19, the computational analysis for the proposed LECA and CyFlaP resulted in the following results. The Magnus effect on the LECA and CyFlaP is demonstrated in Figures 12 to 19 by injecting a momentum injection of 500 RPM and 1000 RPM, respectively. In all cases for this analysis, the cylinder rotation was set on all the CFD simulations examined, rotating in the clockwise direction. The planned environment was to uphold the momentum injection on the aerofoil's upper surface aligned with the free streamflow's path.

Figures 12 and 13 present the aerodynamic performance of the Magnus effect on LECA at 500 RPM. Here, the performance of the LECA was increased at $\alpha = 0°$ for 5 m/s to 10 m/s conditions yet still had some aerodynamic performance below the unmodified model from Selig at higher α for 15 m/s to 30 m/s conditions (Selig et al., 1995; Selig et al., 1996). Despite this variance, the application of cylinders at both sides of the aerofoil has resulted in slight C_L improvement. Next, the 5 m/s conditions have resulted in a 53% stall angle delay at $\alpha = 20°$ beyond the unmodified model. The help of flow recovery at low wind speed may be the one that contributed the most to this model condition. However, the lowest C_L can be seen at $\alpha = 20°$ with a 37% coefficient below the unmodified model for 15 m/s conditions, where it was caused predominantly by the shape of the aerofoil, which formed high separation and burbling at the aftward surfaces of the aerofoil as the flow broke away that clearly shows the reason of high C_D as seen in Figure 13. Therefore, it can be denoted that the LECA behaved the best at a higher α for lower wind velocity. A higher rotational speed would amplify the recovery of depleted C_L at the lower α later.

Figures 14 and 15 display the aerodynamic performance of the Magnus effect on LECA at 1000 RPM. The trends showed better C_L for lower freestream flow but not for larger value of freestream flow. For lower freestream flow, i.e., 5 m/s, LECA generates higher C_L and lower C_D than the rest of the free stream velocities, which has 39% better C_{Lmax}

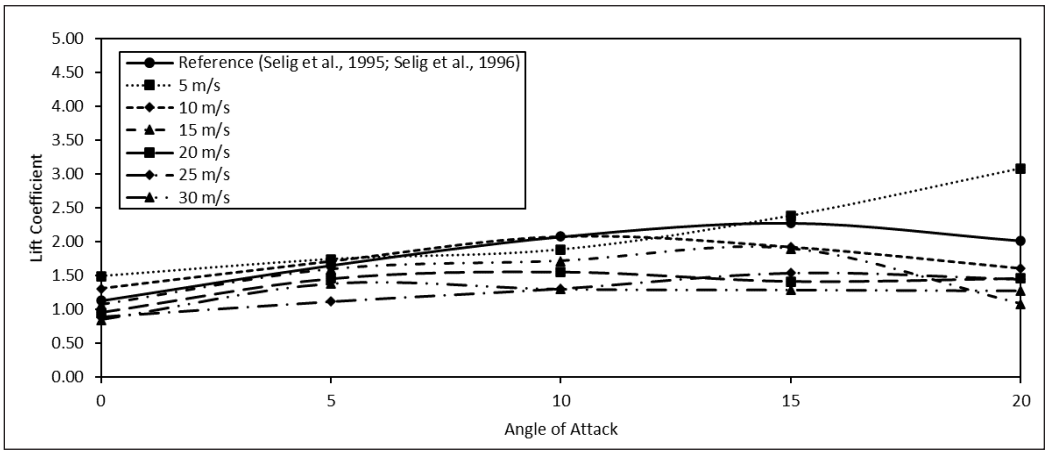

Figure 12. C_L of LECA versus α at 500 RPM of rotational speed

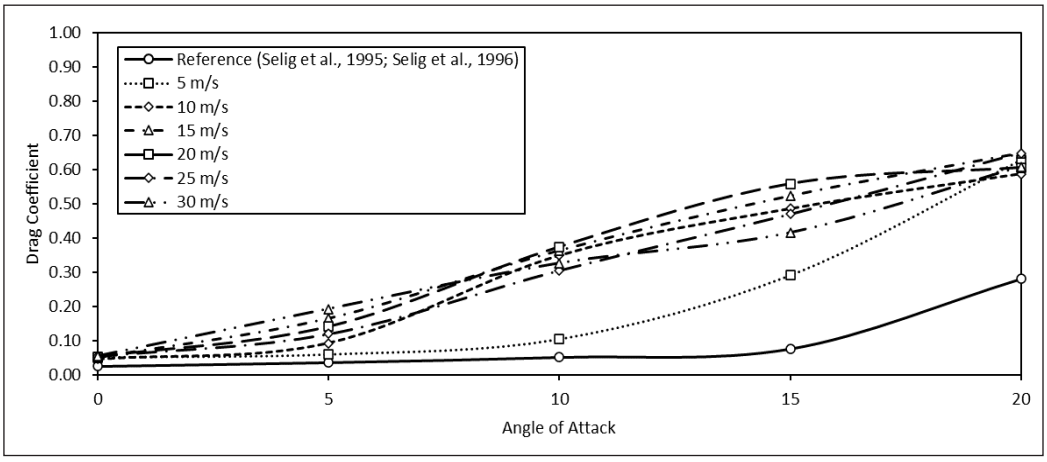

Figure 13. C_D of LECA versus α at 500 RPM of rotational speed

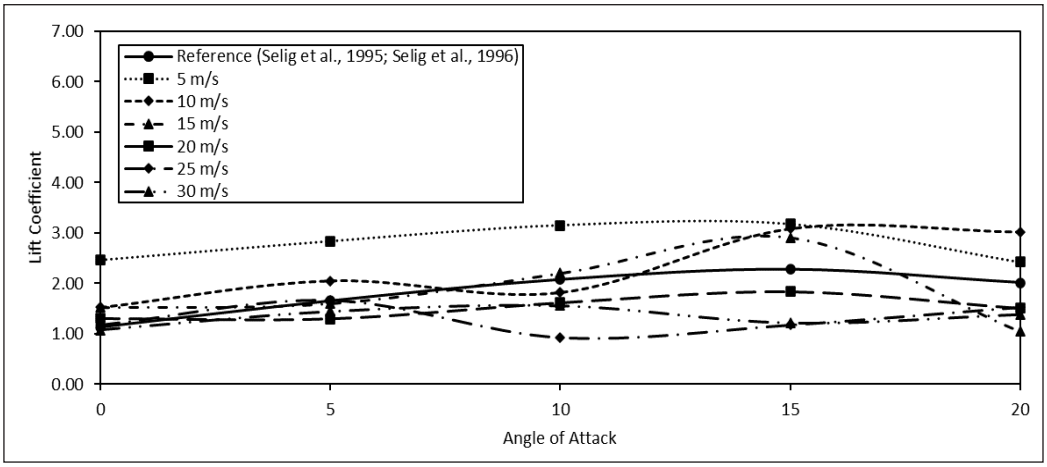

Figure 14. C_L of LECA versus α at 1000 RPM of rotational speed

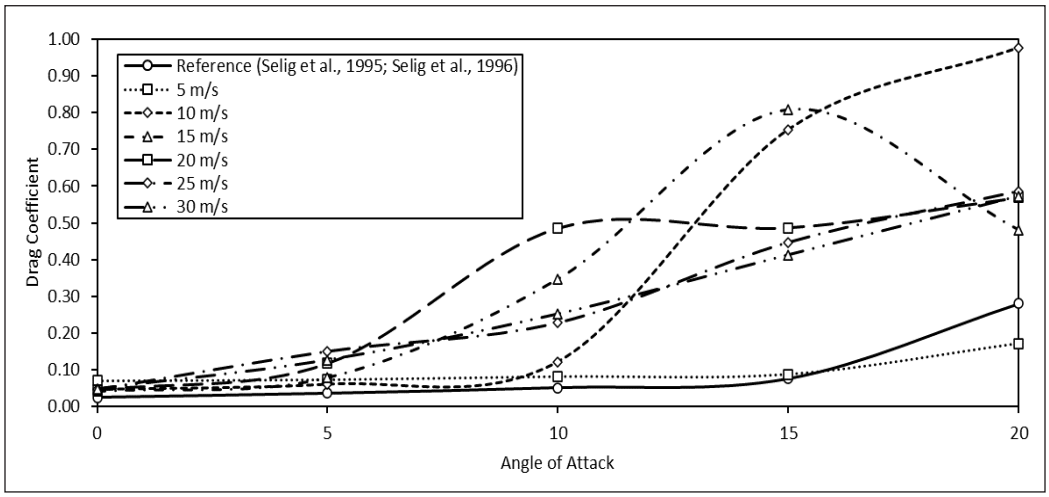

Figure 15. C_D of LECA versus α at 1000 RPM of rotational speed

than the unmodified model at $\alpha = 15°$ before stalling. At a velocity of 10 m/s and 25 m/s, the trend rose then stalled from $\alpha = 5°$ to 10°, yet rose back on higher α onwards. This diminution was caused by a flow separation aftward of the LECA, which was recovered with momentum injection from the trailing edge rotating cylinder. As for LECA at 15 m/s and 20 m/s free stream velocities, a slight plateau effect was seen at the initial flow from $\alpha = 0°$ to 5°. This sudden plateau effect was caused by the gradually reducing aerodynamic coefficient but did not stall immediately. Despite some of the 1000 RPM momentum injections showing better performances against the 500 RPM yet, the high drag effect due to the swirling vortices aftward of the cylinder was not able to recover fully, which has affected the LECA's aerodynamic performance, especially in generating inconsistent C_L. An increase in the cylinder rotational speed may help elevate its aerodynamic performance for certain free stream velocities conditions. However, it may not be suitable for the intended HAP, designed to operate at high altitudes with such inevitable turbulence.

Figures 16 and 17 show the aerodynamic performance of the Magnus effect on CyFlaP at 500 RPM. At this condition, the highest C_L was denoted at 5 m/s conditions with a 128% improvement to the unmodified model. However, the lowest was 26% for 30 m/s free stream velocities. Moreover, a slight plateau effect can be seen at $\alpha = 5°$ to 10°, but the condition may recover with a further increment of momentum injection on the model. Overall, the C_L performance showed satisfactory results beyond the unmodified model (Torres, 2002). Figure 17 showed the C_D of CyFlaP, which showed high values of C_D due to the swirling vortices carried away from the trailing edge section of the model. However, it is significantly better than the LECA's C_D and is on par with the unmodified model C_D. The matter can be resolved with higher momentum injection to elevate its aerodynamic performance, reducing the drag even further.

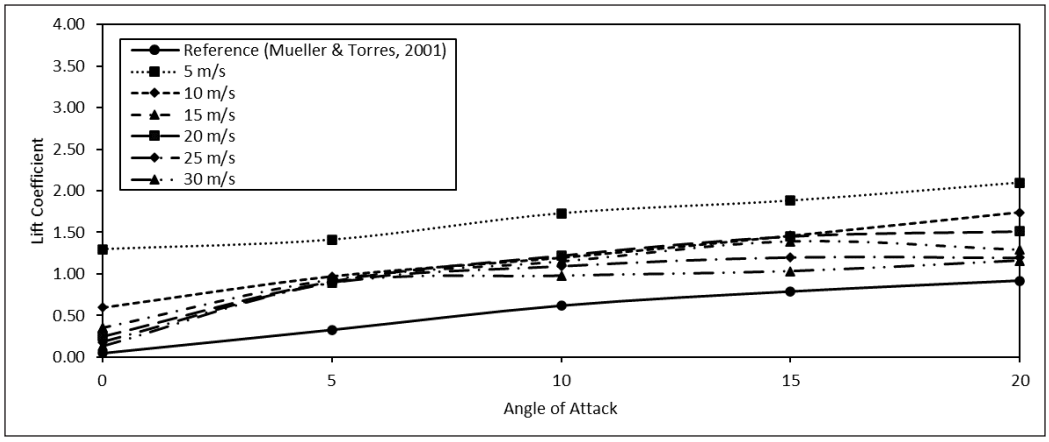

Figure 16. C_L of CyFlaP versus α at 500 RPM of rotational speed

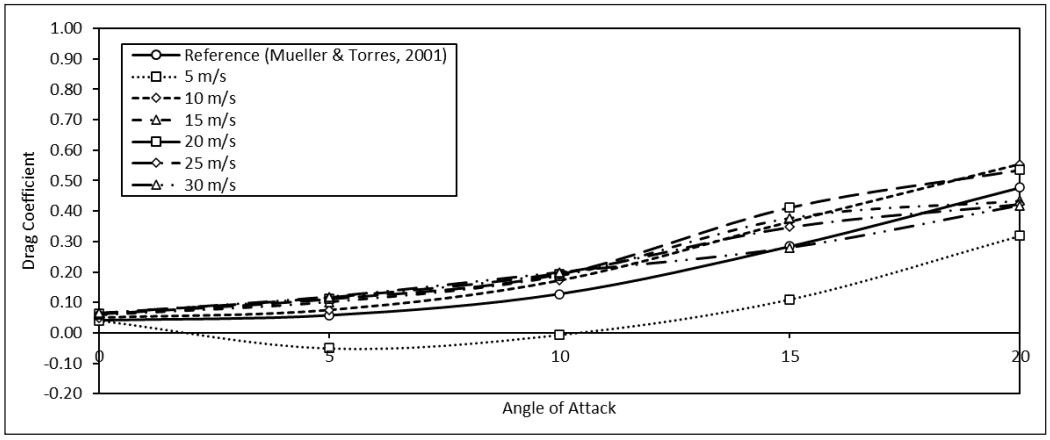

Figure 17. C_D of CyFlaP versus α at 500 RPM of rotational speed

Figures 18 and 19 show the aerodynamic performance of the Magnus effect on CyFlaP at 1000 RPM. The graph trend for CyFlaP is better than LECA embedment, which showed a tremendous effect on all the free stream velocities and α. The freestream velocities of 5 m/s to 15 m/s resulted in a modest increase in performance, which might be attributed to the separation bubble. It recovered for a higher α, which further elevated its aerodynamic coefficient and stall angle delay by up to 204% better than the unmodified model. Based on this trend, the CyFlaP may go for a higher α beyond the $\alpha = 20°$. The negative C_D trend in Figures 17 and 19 is equivalent to a positive thrust which resulted in a high C_L value recorded. Nevertheless, for higher free stream velocities of 20 m/s to 30m/s, the trend showed an increase in C_L yet plateau from $\alpha = 5°$ to 15°. The same plateau effect from LECA and CyFlaP is due to the partial separation bubble during the flight. However, it may be recovered with an increment of the momentum injection, which helps reattach the air stream towards the LECA and CyFlaP surface body.

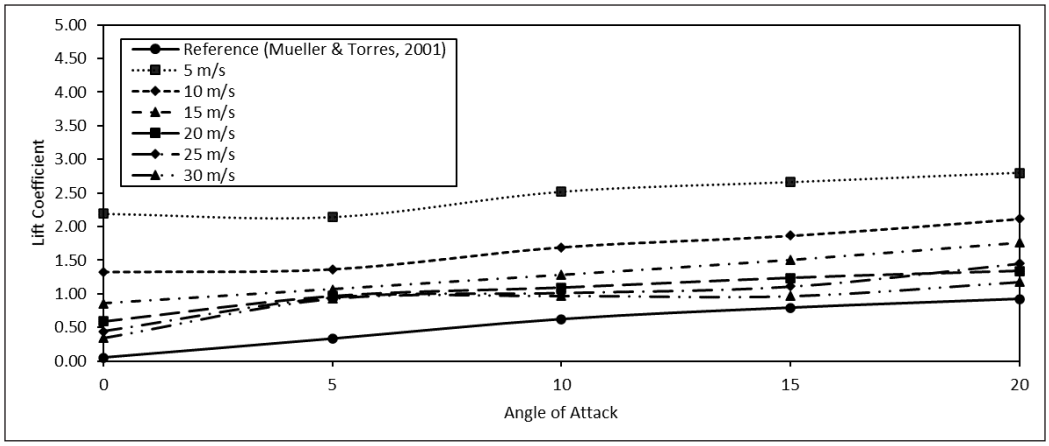

Figure 18. C_L of CyFlaP versus α at 1000 RPM of rotational speed

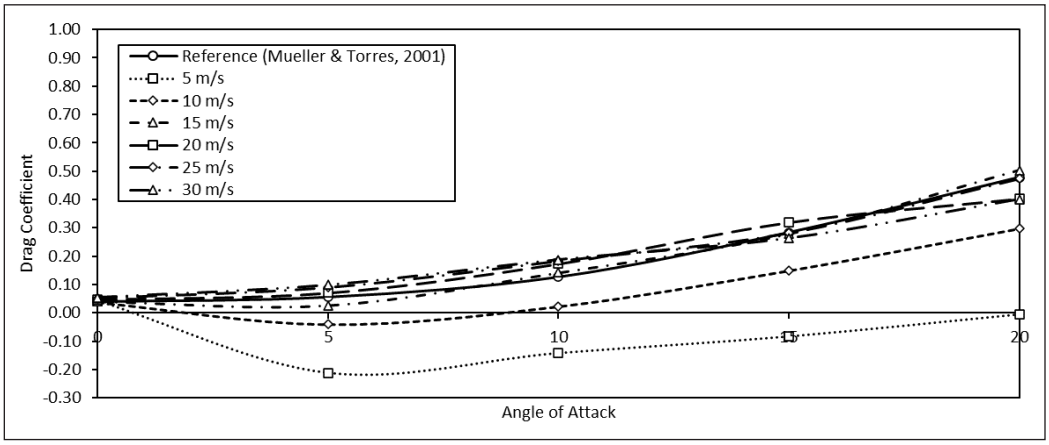

Figure 19. C_D of CyFlaP versus α at 1000 RPM of rotational speed

Comparatively, the unmodified Selig S1223 aerofoil has better C_L than the unmodified flat plate in terms of aerodynamic performance. In this case, the momentum injection for the flat plate, known as the CyFlaP, works well in attaining its aerodynamic coefficient and is thus more stable and suitable for the application of HAP than the modified LECA. Furthermore, the wobble in the LECA trend may not be suitable for HAP as this may be dangerous and difficult to control at such a high altitude. Previously, the highest recorded data on the leading-edge cylinder embedment has a maximum lift of 145% for NACA 0010 aerofoil by Huda et al. (2015), followed by 36% in C_L by Ahmed et al. (2014). On the contrary, this research study has proved that the LECA generated 39% and 53% improvement while the CyFlaP has denoted 128% and 204% enhancement on its C_L and stall angle delay, respectively. These recorded data clearly show that the use of double rotating cylinders on both designs would be beneficial in stabilizing its aerodynamic performance, especially

on the CyFlaP, where the coefficient may extend beyond the recorded α. Finally, it should be noted that the LECA and CyFlaP designs perform better at lower free stream velocities, which are appropriate for the stratosphere region.

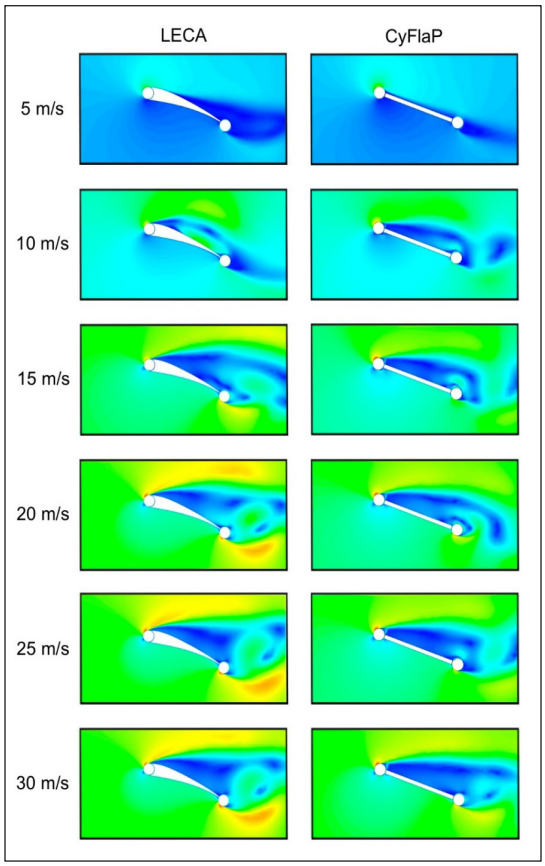

Figure 20. Velocity magnitude contour on LECA (Left) and CyFlaP (Right) at $\alpha = 20°$

Effect on Velocity Magnitude Contour. The flow evolution was derived from the CFD post-processing for this investigation. The velocity inlet of 5 m/s to 30 m/s was used to express the physical vector quantity. For free stream velocities of 5 m/s to 30 m/s at 1000 RPM, the velocity magnitude contour for twelve (12) different conditions at $\alpha = 20°$ is shown in Figure 20. Here, partial flow separation can be seen behind the LECA and smooth flow contour for the CyFlaP at 5 m/s free stream velocity. A higher value of free stream velocities resulted with flow separation starting from 10 m/s onwards, where a swirling vortex started to occur aftward of the model. Meanwhile, the trailing edge rotating cylinder momentum injection aids in reattaching the flow to the surface before catastrophic phenomena such as stall occur. A higher momentum injection would be suggested to study the flow reattachment as moving surface boundary control. Flow reattachment would be sufficient to bring the stable flight back into its path for HAP application.

Effect on Pressure Coefficient Contour. Another set of flow evolution for pressure coefficient (C_p) was derived from the CFD post-processing to study its pressure distribution along the surface body of the model, as shown in Figure 21. This analysis represented 12 conditions for free stream velocities ranging from 5 to 30 m/s at 1000 RPM momentum injection at $\alpha = 20°$. Here, the partial flow separation from the previous clause indicates the existence of Kármán vortex street. Furthermore, it was a condition in which swirling vortices emerge aftward the model, affecting the present flow over time. In Figures 20 and 21, a larger formation of swirling vortices can be seen aftward of the LECA, which

may be the factor with the wobble for its aerodynamic coefficient, resulting in high C_D, which may cause vibration and inconsistent flight.

Based on Bernoulli's principle, low pressure on the upper surface and higher pressure on the lower surface body resulted in higher lift and lower drag generation. The rotation of the rotating cylinder is further enhanced, thus reattaching the flow onto its surface body whenever flow separation occurs. Furthermore, a formation of higher pressure was depicted towards the lower rotating cylinder surfaces with an increment of free stream velocities, concluding upon the success of Magnus effect generation for the model's embedment in HAP application. Therefore, a momentum injection played a vital role in improving the flow boundary layer back onto its surface body. Therefore, a higher momentum injection is suggested to reattach the flow further, thus reducing its drag generation.

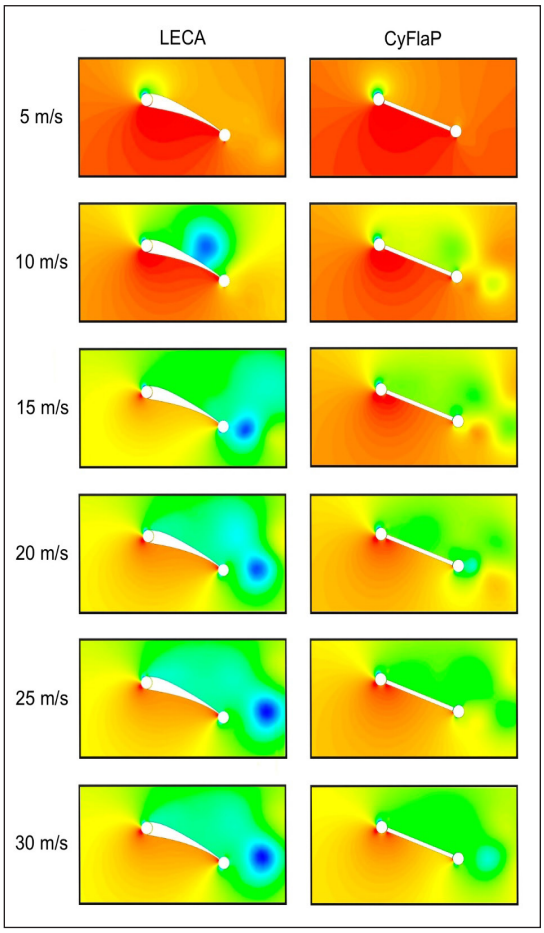

Figure 21. C_p contour on LECA (Left) and CyFlaP (Right) at $\alpha = 20°$

CONCLUSION

The numerical simulation analysis by embedding rotating cylinders onto LECA and CyFlaP has tremendously affected their aerodynamic coefficients. The analysis yielded the effects on C_L and stall angle delay of about 39% and 53%, respectively, for LECA while showing 128% and 204% better for CyFlaP than their respective unmodified model. It is believed that the CyFlaP provides more stability while being simple in design, making it appropriate for HAP applications. Despite having a better aerodynamic coefficient than the CyFlaP, the LECA is unsuitable for the task due to uneven flow and excessive vortices. The momentum injection on the model showed a rise in C_L, reduction in C_D, and yet extended its stall angle delay, thus concluded upon the successful Magnus effect application on the model. Overall, further research, such as momentum injection increment, will be recommended to improve its aerodynamic performance for the intended HAP application.

ACKNOWLEDGEMENT

The Ministry of Education (MoE) Malaysia supported this research under the research grant scheme of Fundamental (FRGS) Phase 1/2018 with MoE ref. code FRGS/1/2018/TK09/UPM/02/2 and project code of 03-01-18-1950FR. The support is gratefully acknowledged.

REFERENCES

Abdulla, N. N., & Hasan, M. F. (2018). Effect of gap between airfoil and embedded rotating cylinder on the airfoil aerodynamic performance. *Research & Development in Material Science, 3*(4), 1-10. https://doi.org/10.31031/rdms.2018.03.000567

Ahmed, S., Nazari, A., & Wahba, E. (2014). Numerical analysis of separation control over an airfoil section. *International Review of Aerospace Engineering, 7*(2), 61-68. https://doi.org/10.15866/irease.v7i2.2057

Ali, H. M., Rafie, A. S. M., Ali, S. A. M., & Gires, E. (2021a). Computational analysis of the rotating cylinder embedment onto flat plate. *CFD Letters, 13*(12), 133-149. https://doi.org/10.37934/cfdl.13.12.133149

Ali, H. M., Rafie, A. S. M., & Ali, S. A. M. (2021b). Numerical analysis of leading-edge cylinder aerofoil on Selig S1223 for moving surface boundary control. *Journal of Aeronautics, Astronautics and Aviation, 53*(2), 143-153. https://doi.org/10.6125/JoAAA.202106_53(2).06

ANSYS. (2013) *ANSYS fluent theory guide*. ANSYS, Inc. https://www.academia.edu/38091499/ANSYS_Fluent_Theory_Guide

Badalamenti, C., & Prince, S. (2008). *Effects of endplates on a rotating cylinder in crossflow*. In *AIAA Applied Aerodynamics Conference*. American Institute of Aeronautics Ins. https://doi.org/10.2514/6.2008-7063

Barati, E., Zarkak, M. R., & Esfahani, J. A. (2019, April 30 - May 2). *Effect of rotational direction of circular cylinder for mixed convection at subcritical Reynolds Number*. In *27th Annual International Conference of Iranian Society of Mechanical Engineers (ISME 2019)* (pp. 1-6). Tehran, Iran.

Boye, T. E., Nwaoha, T. C., Olusegun, S. D., & Ashiedu, F. I. (2017). A validation method of computational fluid dynamics (CFD) simulation against experimental data of transient flow in pipes system. *American Journal of Engineering Research*, *6*(6), 67-79.

Chunchuzov, I., Kulichkov, S., Perepelkin, V., Popov, O., Firstov, P., Assink, J. D., & Marchetti, E. (2015). Study of the wind velocity-layered structure in the stratosphere, mesosphere, and lower thermosphere by using infrasound probing of the atmosphere. *Journal of Geophysical Research: Atmosphere, 120*(17), 8828-8840. https://doi.org/10.1002/2015JD023276

D'Oliveira, F. A., Melo, F. C. L. D., & Devezas, T. C. (2016). High-altitude platforms - Present situation and technology trends. *Journal of Aerospace Technology and Management*, *8*(3), 249-262. https://doi.org/10.5028/jatm.v8i3.699

Faisal, K. M., Salam, M. A., Ali, M. T., Sarkar, M. S., Safa, W., & Sharah, N. (2017). Flow control using moving surface at the leading edge of aerofoil. *Journal of Mechanical Engineering, 47*(1), 45-50. https://doi.org/10.3329/jme.v47i1.35420

Fidler, F., Knapek, M., Horwath, J., & Leeb, WR. (2010). Optical communications for high-altitude platforms. *Journal of Selected Topics in Quantum Electronics*, *16*(5), (1058-1070). https://doi.org/10.1109/JSTQE.2010.2047382

Gowree, E. R., & Prince, S. A. (2012). A computational study of the aerodynamics of a spinning cylinder in a crossflow of high Reynolds number. In *Proceedings of the 28th Congress of the International Council of the Aeronautical Sciences (ICAS'12)* (pp. 1138-1147). Academia.

Gultom, A., & Yuniarti, D. (2016). Kajian teknologi high altitude platform (HAP) [Study of high altitude platform (HAP) technology]. *Buletin Pos Dan Telekomunikasi*, *14*(1), 1-11. https://doi.org/10.17933/bpostel.2016.140102

Hamisu, M. T., Jamil, M. M., Umar, U. S., & Sa'ad, A. (2019). Numerical study of flow in asymmetric 2D plane diffusers with different inlet channel lengths. *CFD Letters, 11*(5), 1-21.

Huda, M. N., Ahmed, T., Ahmed, T. S. M., Salam, M. A., Afsar, M. R., Faisal, K. M., & Ali, M. T. (2015). *Study of NACA 0010 symmetric airfoil with leading edge rotating cylinder in a subsonic wind tunnel*. ResearchGate.

Khalil, H., Saqr, K., Eldrainy, Y., & Abdelghaffar, W. (2018). Aerodynamics of a trapped vortex combustor: A comparative assessment of RANS based CFD models. *Journal of Advanced Research in Fluid Mechanics and Thermal Sciences, 43*(1), 1-19.

Khan, S. A., Bashir, M., Baig, M. A. A., & Ali, F. A. G. M. (2020). Comparing the effect of different turbulence models on the CFD predictions of NACA0018 airfoil aerodynamics. *CFD Letters, 12*(3), 1-10. https://doi.org/10.37934/cfdl.12.3.110

Kim, S. E., Choudhury, D., & Patel, B. (1999). Computations of complex turbulent flows using the commercial code FLUENT. In M. D. Salas, J. N. Hefner & L. Sakell (Eds.), *Modeling complex turbulent flows* (pp. 259-276). Springer. https://doi.org/10.1007/978-94-011-4724-8_15

Kölzsch, A., & Breitsamter, C. (2014). Vortex-flow manipulation on a generic delta-wing configuration. *Journal of Aircraft, 51*(5), 1380-1390. https://doi.org/10.2514/1.C032231

Menter, F. R. (1994). Two-equation eddy-viscosity turbulence models for engineering applications. *AIAA Journal*, *32*(8), 1598-1605. https://doi.org/10.2514/3.12149

Merryisha, S., & Rajendran, P. (2019). *CFD validation of NACA 2412 airfoil*. ResearchGate. https://doi.org/10.13140/RG.2.2.16245.42723

Mgaidi, A. M., Rafie, A. S., Ahmad, K. A., Zahari, R., Hamid, M. F. A., & Marzuki, O. F. (2018). Numerical and experimental analyses of the flow around a rotating circular cylinder at subcritical regime of Reynolds number using K-E and K-Ω-SST turbulent models. *ARPN Journal of Engineering and Applied Sciences*, *13*(3), 954-960.

Modi, V. J. (1997). Moving surface boundary-layer control: A review. *Journal of Fluids Structures*, *11*(6), 627-663. https://doi.org/10.1006/jfls.1997.0098

Modi, V. J., Fernando, M. S. U. K., & Yokomizo, T. (1991). Moving surface boundary-layer control-Studies with bluff bodies and application. *AIAA Journal*, *29*(9), 1400-1406. https://doi.org/10.2514/3.10753

Monk, D., & Chadwick, E. A. (2017, July 3-6). *Comparison of turbulence models effectiveness for a delta wing at low Reynolds numbers*. In *7th European Conference for Aeronautics and Space Sciences (EUCASS)* (pp. 1-12). Milan, Italy. https://doi.org/10.13009/EUCASS2017-653

Oller, S. A., Nallim, L., & Oller, S. (2016). Usability of the Selig S1223 profile airfoil as a high lift hydrofoil for hydrokinetic application. *Journal of Applied Fluid Mechanics (JAFM), 9*(2), 537-542. https://doi.org/10.18869/acadpub.jafm.68.225.24302

Russo, F., & Basse, N. T. (2016). Scaling of turbulence intensity for low-speed flow in smooth pipes. *Flow Measurement and Instrumentation, 52,* 101-114. https://doi.org/10.1016/j.flowmeasinst.2016.09.012

Salam, M. A., Deshpande, V., Khan, N. A., & Ali, M. T. (2019). Numerical analysis of effect of leading-edge rotating cylinder on NACA0021 symmetric airfoil. *European Journal of Engineering and Technology Research, 4*(7), 11-17. https://doi.org/10.24018/ejeng.2019.4.7.1385

Selig, M. S., & Guglielmo, J. J. (1997). High-lift low Reynolds number aerofoil design. *Journal of Aircraft*, *34*(1), 72-79. https://doi.org/10.2514/2.2137

Selig, M. S., Guglielmo, J. J., Broeren, A. P., & Gigue´re, P. (1995). *Summary of low-speed airfoil data, Volume 1*. SoarTech Publications.

Selig, M. S., Lyon, C. A., Gigue´re, P., Ninham, C. P., & Guglielmo, J. J. (1996). *Summary of low-speed airfoil data*, *Volume 2*. SoarTech Publications.

Šidlof, P., Antoš, P., Šimurda, D., & Štěpán, M. (2017). Turbulence intensity measurement in the wind tunnel used for airfoil flutter investigation. *EPJ Web of Conferences, 143*, Article 02107.https://doi.org/10.1051/epjconf/201714302107

Torres, G. E. (2002). *Aerodynamics of low aspect ratio wings at low Reynolds numbers with applications to micro air vehicle design and optimization* (Publication No. 3040583). (Doctoral dissertation). University of Notre Dame, USA. https://www.proquest.com/docview/305522704?pq-origsite=gscholar&fromopenview=true

Tozer, T., & Grace, D. (2001). High-altitude platforms for wireless communications. *IEE Electronics & Communication Engineering Journal, 13*(3), 127-137. https://doi.org/10.1049/ecej:20010303

Wang, S., Zhang, X., He, G., & Liu, T. (2013). A lift formula applied to low-Reynold-number unsteady flows. *Physics of Fluid*, *25*, Article 093605. https://doi.org/10.1063/1.4821520

Wilcox, D. C. (1988). Reassessment of the scale-determining equation for advanced turbulence models. *American Institute of Aeronautics and Astronautics Journal*, *26*(11), 1299-1310. https://doi.org/10.2514/3.10041

Wolff, E. B. (1925). *Preliminary investigation of the effect of a rotating cylinder in a wing* (No. NACA-TM-307). National Advisory Committee for Aeronautics. https://ntrs.nasa.gov/api/citations/19930086915/downloads/19930086915.pdf

Yao, Q., Zhou, C. Y., & Wang, C. (2016). Numerical study of the flow past a rotating cylinder at supercritical Reynolds number. In *Proceedings of the 2016 4th International Conference on Mechanical Materials and Manufacturing Engineering* (p. 813-816). Atlantis Press. https://doi.org/10.2991/mmme-16.2016.159